

## Convective Heat Transfer Inside Rotating Tubes

S. Chakravarthy, T.K. Bose, P. Batten, S. Palaniswamy, U. Goldberg and O. Perroomian  
*Metacomp Technologies, Inc., Westlake Village, CA 91361*

### ABSTRACT

An unstructured finite volume code employing a non-linear eddy-viscosity turbulence closure is applied to the study of the internal flow through a square passage containing a 180° U-bend. The tube walls are heated to represent the internal walls of a turbine-blade cooling passage. Both stationary and rotating tubes are considered. Three cases were chosen to match available experimental and computational data: the Reynolds number of each case was  $10^5$  based on bulk velocity and hydraulic diameter and rotation numbers were 0, +0.2 (counter-clockwise rotation) and -0.2 (clockwise rotation). The present turbulence model displays broad agreement with previous ASM computations, including similar discrepancies with data downstream of separation in the U-bend.

### NOMENCLATURE

$c_p$	- specific heat of air, J/(kg.K)
$D$	- hydraulic diameter, m
$E$	- total energy per unit mass, J/kg
$k$	- turbulent kinetic energy, $m^2/s^2$
$Nu$	- Nusselt number = $\alpha D / \lambda_{wall}$
$\mathbf{q}$	- heat-flux vector, $W/m^2$
$P_k$	- turbulence production, $m^2/s^3$
$Re$	- Reynolds number = $\rho V_b D / \mu$
$Ro$	- rotation number = $\Omega D / V_b$
$r$	- radius, m
$\mathbf{S}$	- mean-strain tensor
$T$	- temperature, K
$t$	- time, s
$U$	- mean velocity, m/s
$u$	- velocity fluctuation, m/s
$V_b$	- bulk (inlet) velocity, m/s
$\mathbf{W}$	- mean-vorticity tensor
$X_i$	- vector to axis of rotation
$x$	- length coordinate, m
$\alpha$	- heat transfer coefficient = $q_{wall} / (T_{inlet} - T_{wall})$ , $W/(m^2K)$
$\varepsilon$	- turbulence dissipation rate, $m^3/(kg.s)$
$\varepsilon_{ijk}$	- third-order alternating tensor
$\phi$	- stagger angle
$\lambda$	- heat con. coefficient, $W/(m.K)$
$\mu$	- dynamic viscosity coeff., $kg/(m.s)$
$\mu_t$	- turb. eddy viscosity, $kg/(m.s)$
$\rho$	- density, $kg/m^3$
$\theta$	- U-bend angle
$\tau$	- shear stress, $N/m^2$

$\Omega$  - angular velocity, rad./s

$(\bar{\quad})$  - time-averaged quantities

### INTRODUCTION

The requirement for designing efficient jet engines with large thrust-to-weight ratios in modern jet engines generally results in higher turbine inlet temperatures, which necessitates an effective cooling of various rotating turbine components (Fig. 1). Although the cooling of several components may be required, one of the most critical components is the turbine blade<sup>1-5</sup>. Internal cooling passages are typically employed, whose surfaces are often augmented with devices such as fins, ribs and other artificial surface-roughening aids in order to enhance turbulent mixing and hence heat transfer.

This paper presents a study of the flow through an internal tubular passage with a U-bend which is either stationary or rotating about an axis perpendicular to the plane of the U-bend (Fig. 2). Normally, the stagger angle is parallel to the chord of the blade or equal to the tangent to camber line at that point. However, a specific geometry has been chosen here, similar to the one used in experiments by Cheah et al.<sup>6</sup> and for this purpose, the tubular passage was of square cross-section and calculations were done for  $\theta = 90^\circ$  (orthogonal mode rotation).

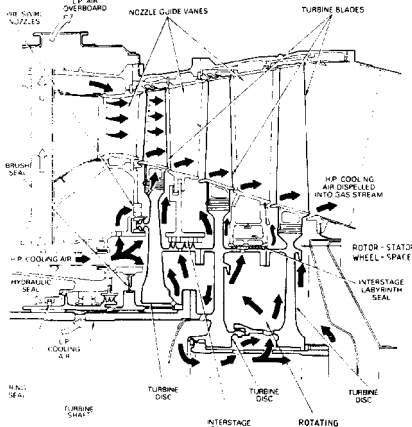


Fig. 1 Schematic of cooling-air path through rotating turbine components  
(by permission of Rolls-Royce Ltd)

The coolant gas is constrained to flow through a 180° U-bend, where it is subjected to effects of strong streamline curvature, wall heating (and hence centripetal forces due to density variations within the fluid) and Coriolis forces. These forces influence the mean flow directly and also indirectly through influences on the fluctuating velocity components and are therefore known to alter the mean-flow behavior and the turbulence-enhanced heat transfer rates. Secondary motion induced by curvature, centripetal and Coriolis forces, for example, are expected to have a beneficial effect by increasing the mixing rate, however, turbulent production rates may be either augmented or diminished according to the relative orientation of the flow vector with respect to the acceleration vector.

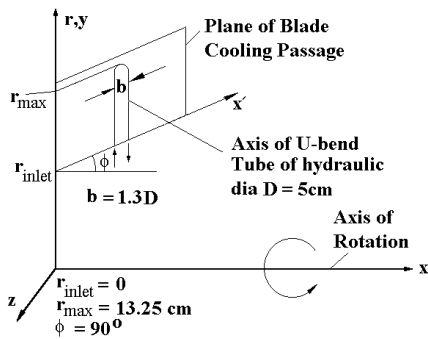


Fig. 2 Selected geometry

## GOVERNING EQUATIONS AND NUMERICAL MODELING

The basic equations of the mean flow consist of the continuity, momentum and energy equations, with an assumption of ideal gas and the appropriate rotation terms:

$$\frac{\partial \bar{\rho}}{\partial t} + \frac{\partial (\bar{\rho} U_k)}{\partial x_k} = 0 \quad (1a)$$

$$\begin{aligned} \frac{\partial (\bar{\rho} U_i)}{\partial t} + \frac{\partial (\bar{\rho} U_i U_k)}{\partial x_k} = & -\frac{\partial \bar{p}}{\partial x_i} + \frac{\partial}{\partial x_k} [\bar{\tau}_{ik} - \overline{\rho u_i u_k}] \\ & - 2\bar{\rho} \varepsilon_{ipk} \Omega_p U_k - \bar{\rho} (\Omega_k X_k \Omega_i - \Omega_k X_i \Omega_k) \\ \frac{\partial (\bar{\rho} E)}{\partial t} + \frac{\partial (\bar{\rho} E + \bar{p}) U_k}{\partial x_k} = & -\frac{\partial}{\partial x_k} (c_p \bar{\rho} T'' u_k + \bar{q}_k) \\ & + \frac{\partial}{\partial x_k} (-\bar{\rho} U_i u_i u_k + U_i \bar{\tau}_{ik}) \\ & + \frac{\partial}{\partial x_k} \left( -\frac{1}{2} \overline{\rho u_j u_j u_k} + \overline{u_j \tau_{jk}} \right) \\ & + U_i [-2\bar{\rho} \varepsilon_{ipk} \Omega_p U_k - \bar{\rho} (\Omega_k X_k \Omega_i - \Omega_k X_i \Omega_k)] \end{aligned} \quad (1b,c)$$

The computations were performed using a finite-volume flow-simulation software package, CFD++. CFD++ can deal with arbitrary mesh types, including multi-block, patched and overset meshes. It handles these accurately through the use of formally second-order accurate multi-dimensional interpolation generalized to include all possible cell topologies. CFD++ was used here with the following options:

- A multi-dimensional TVD interpolation to ensure a bounded convection scheme
- A non-linear Riemann solver (HLLC) to ensure positivity and obviate the need for entropy corrections
- Implicit time-stepping with algebraic multigrid acceleration

## TURBULENCE MODELING

Turbulence closure was provided by means of a non-linear eddy-viscosity model. Whilst this model cannot exactly represent the modifications to the turbulence production rate due to Coriolis and centripetal forces (these contributions have zero trace), the model is able to give some representation of normal-stress anisotropy,

streamline curvature and bulk rotation effects. The model consists of transport equations for  $k$  and  $\varepsilon$  and an expansion for the anisotropy tensor involving terms up to, and including those, cubic in the mean strain and vorticity tensors. The turbulent transport equations are as follows:

$$\begin{aligned} & \frac{\partial(\bar{\rho}k)}{\partial t} + \frac{\partial(\bar{\rho}U_k k)}{\partial x_k} \\ &= \frac{\partial}{\partial x_k} \left[ \left( \mu + \frac{\mu_t}{\sigma_k} \right) \frac{\partial k}{\partial x_k} \right] + P_k - \bar{\rho}\varepsilon \\ & \frac{\partial(\bar{\rho}\varepsilon)}{\partial t} + \frac{\partial(\bar{\rho}U_k \varepsilon)}{\partial x_k} = \frac{\partial}{\partial x_k} \left[ \left( \mu + \frac{\mu_t}{\sigma_\varepsilon} \right) \frac{\partial \varepsilon}{\partial x_k} \right] \\ & + (c_{\varepsilon 1} P_k - c_{\varepsilon 2} \bar{\rho}\varepsilon + E) T_t^{-1} \end{aligned} \quad (1d-e)$$

in which

$$T_t = \frac{k}{\varepsilon} \max\{1, \xi^{-1}\}$$

where  $\xi = \sqrt{R_t/2}$  with  $R_t = \rho k^2 / (\mu\varepsilon)$ .

The Reynolds-stress tensor is then modeled as:

$$\begin{aligned} \frac{u_i u_j}{k} &= \frac{2}{3} \delta_{ij} + a_0 S_{ij} + a_1 \left( \mathbf{S}^2 - \frac{1}{3} \mathbf{S}^2 \mathbf{I} \right) \\ &+ a_2 (\mathbf{W}\mathbf{S} - \mathbf{S}\mathbf{W}) + a_3 \left( \mathbf{W}^2 - \frac{1}{3} \mathbf{W}^2 \mathbf{I} \right) \\ &+ (b_1 \mathbf{S}^2 + b_2 \mathbf{W}^2) \mathbf{S} \\ &+ b_3 \left( \mathbf{W}^2 \mathbf{S} + \mathbf{S}\mathbf{W}^2 - \frac{2}{3} \{ \mathbf{S}\mathbf{W}^2 \} \mathbf{I} \right) \\ &+ b_4 (\mathbf{W}\mathbf{S}^2 - \mathbf{S}^2 \mathbf{W}) \end{aligned}$$

$$\text{where } S_{ij} = \frac{k}{\varepsilon} \left( \frac{\partial U_i}{\partial x_j} + \frac{\partial U_j}{\partial x_i} \right)$$

and the vorticity tensor, now modified due to the bulk rotation, is given by:

$$\Omega_{ij} = \frac{k}{\varepsilon} \left( \frac{\partial U_i}{\partial x_j} - \frac{\partial U_j}{\partial x_i} - \varepsilon_{ijk} \Omega_k \right).$$

Full details of this model, including all model terms and constants can be found in Goldberg et al<sup>14</sup>.

## RESULTS

Experiments, performed previously on these geometries by Cheah et al.<sup>6</sup>, consisted of a square duct of hydraulic diameter (one side of the duct) 5cm, with inner and outer radii of curvature corresponding to 3.25cm and 0.75cm respectively. The distance from the outer wall to the axis of rotation was 13.25cm. The Rotation number of 0.2 corresponded in our computations to 143 radians/second, or 1366 rpm. The axis of rotation was parallel to the axis of curvature of the U-bend and the plane of rotation was horizontal (rotation vector considered vertically upward). Both positive (here defined as counter-clockwise) and negative rotation was considered. (Note that Cheah et al.<sup>6</sup> consider *clockwise rotation as positive*.) In these experiments, the fluid medium was water. The present computations pertain to gas flows and the possibility of a heated gas, which can alter the molecular viscosity and hence the local Reynolds number. The inlet (cooling) air temperature was taken as 300K and computations were done with both cooled (300K) and heated (700K) walls. The bulk velocity at inlet was taken as 35.78m/s and a back pressure of one atmosphere was imposed at the outlet. The Reynolds number (based on inlet flow properties and hydraulic diameter) was equal to  $10^5$ .

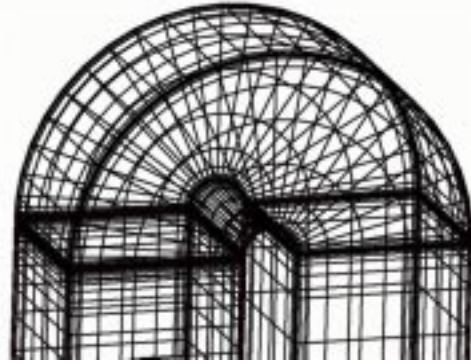


Fig. 3 Grid of U-bend with alternate lines removed for clarity.

The hexahedral grid for the U-bend geometry is shown in Fig. 3, with every other line removed for clarity. The grid consisted of 44x44 points in the cross-

section, with 50 points upstream of the U-bend, 70 points around the elbow of the U-bend itself and 80 points downstream of the bend exit. The grid was clustered to the walls to ensure a  $y^+$  less than 0.5 for all off-wall centroids. The grid was also clustered in the vicinity of the U-bend and in the section immediately downstream of the bend exit.

### **STATIONARY U-BEND**

In order to compare with available data, flow in a stationary U-bend was considered initially. While the inlet gas temperature was always kept at 300K, two wall temperatures, of 300K and 700K were considered. The former was chosen to be more representative of the (incompressible flow) experimental data of Cheah et al<sup>6</sup>; the latter was chosen as a more realistic gas turbine-blade environment. Fig. 4 shows the residual history of all flow variables, indicating that about 360 time-steps are required for a converged solution. The turbulence kinetic energy and streamlines are shown on the symmetry plane (midway in the lateral direction) in Fig. 5. The flow is observed to separate around the 90° section and reattach approximately two diameters downstream of the bend exit. The turbulence levels tend to be suppressed on the outer sides of the tube due to streamwise flow acceleration. The cross-flow pattern in the inlet and return pipe at two diameters upstream and downstream, are shown in Figs. 6a and 6b, respectively. The adverse pressure gradient at the elbow of the U-bend is seen to generate secondary motion downstream of the bend exit. Figs. 7(a-d) show the streamwise velocity distribution of the flow (at both wall temperatures), compared with experiment. These results show a definite effect of density distribution, with the “constant density” case showing closer agreement with experimental results.

Figs. 8(a-c) show the cross-stream velocity distribution at the U-bend entry, mid-section and exit. Figs. 9(a-c) show the turbulence shear-stress distributions at the bend mid-section (90°), exit section and one diameter

downstream. Fig. 9b shows that the predicted shear-stress has the wrong sign at the bend exit – a discrepancy that leads to the insufficient separation observed in the velocity profiles at the same location. This deficiency was previously noted in all models (including ASM’s) tested by Iacovides et al<sup>8</sup>. The Nusselt number,  $\alpha D/\lambda_{wall}$ , is obtained from the wall heat flux:

$$q_{wall} = -\lambda_{wall}(\nabla T)_{wall} = \alpha(T_{inl.} - T_{wall}) \quad (2)$$

Fig. 10 illustrates the surface Nusselt-number distribution, showing the peak heat transfer to occur on the upper and lower walls beyond the bend entry.

### **ANTI-CLOCKWISE ROTATION (Ro=0.2)**

Fig. 11 shows the residual history for the case of counter-clockwise rotation. These residuals show a similar rate of decline, perhaps with some indication of convergence stall, which may be indicative of large-scale unsteady motion. The turbulence kinetic energy and streamlines are shown on the symmetry plane in Fig. 12. Here the Coriolis effect causes the fluid to be forced toward the inner wall, generating a small separation zone near the bend entry on the outer wall. Turbulence levels are also significantly raised, relative to the stationary case, both within and downstream of the bend exit. The cross-flow pattern in the inlet and return pipe at two diameters upstream and downstream, are shown in Figs. 13a and 13b, respectively. Curiously (since the equations imply symmetry about the lateral mid-plane), the secondary motion in the return-flow pipe displays a significant asymmetry. Fig. 13c illustrates this, showing the path of a single particle originating near the lower wall of the inlet pipe. Figs. 14a, 14b and 14c show the turbulence shear-stress distributions at the bend exit, one and three diameters downstream, respectively. Fig. 14a again shows the shear stress to be predicted with the wrong sign at the bend exit, although predictions appear to recover somewhat downstream. Fig. 15 illustrates the surface Nusselt-number distribution, showing a

somewhat different pattern to that observed in the non-rotating case, with peak heat transfer now occurring toward the bend exit on the outer wall both above and below the symmetry plane.

### ***CLOCKWISE ROTATION*** ( $Ro = -0.2$ )

Fig. 16 shows the residual history for the case of clockwise rotation. These residuals show a slower decline than in either of the previous two cases. The turbulence kinetic energy and streamlines are shown on the symmetry plane in Fig. 17. Here the Coriolis effect causes the fluid to be forced toward the *outer* wall, increasing the length of the separation zone downstream of the bend exit. The cross-flow pattern in the inlet and return pipe at two diameters upstream and downstream, are shown in Figs. 18a and 18b, respectively. Again, an asymmetry is noted about the lateral mid-plane. Fig. 19 illustrates the surface Nusselt-number distribution, again showing a different pattern to that observed in either of the two previous cases. The peak heat transfer now occurs on the outer wall at the symmetry plane.

Finally, Figs. 20 and 21 show a comparison of all Nusselt number distributions at the symmetry plane on the inner and outer wall, respectively. The cases with  $Ro = 0$  and  $Ro = 0.2$ , show the peak heat-transfer to occur at about one diameter downstream of the bend exit, whereas the  $Ro = -0.2$  case shows higher overall levels and a peak on the outer wall occurring within the first  $90^\circ$  section of the U-bend. In all cases, the increased heat-transfer rates persist for a significant distance downstream of the U-bend.

### **SUMMARY AND CONCLUSION**

The Coriolis force is capable of exerting a significant effect on the transport of fluid inside U-bend passages. For non-rotating or counter-clockwise rotating U-bends, the Nusselt number on the mid-plane of the

outer-wall peaks at about one diameter downstream of the bend-exit. In the case of clockwise rotation, a much stronger peak occurs within the first  $90^\circ$  section of the U-bend. On the outer surface, the Nusselt number distribution downstream of the U-bend actually appears to decrease if  $Ro > 0$ . In both the positive and negative rotation cases, an asymmetry was observed in the secondary flow downstream of the U-bend.

### **ACKNOWLEDGEMENT**

The authors would like to thank Dr. Hector Iacovides of UMIST, Department of Mechanical Engineering, for a number of useful communications.

### **REFERENCES**

1. A. Hoselhaus, D.T. Vogel and H. Krain, "Coupling of 3D-Navier-Stokes External Flow Calculations and Internal 3D-Heat Conduction for Cooled Turbine Blades", *Proceedings AGARD Conference on Heat Transfer and Cooling in Gas Turbines*, Antalya (Turkey), 12-16 October 1992, AGARD-CP-527, Paper 40.
2. T. Bo, H. Iacovides and B.E. Launder, "The Prediction of Convective Heat Transfer in Rotating Square Ducts", *VIII Symposium on Turbulent Shear Flows*, Munich (Germany), Sept. 9-11, 1991.
3. W.D. Morris and R. Salemi, "The Effect of Orthogonal-Mode Rotation on Forced Convection in a Circular-Sectioned Tube Fitted with Full Circumferential Transfer Ribs", *Proceedings AGARD Conference on Heat Transfer and Cooling in Gas Turbines*, Antalya (Turkey), 12-16 October 1992, AGARD-CP-527, Paper 11.
4. T. Bo and B.E. Launder, "Turbulent Flow and Heat Transfer in Idealized Blade Cooling Passages", *Proceedings AGARD Conference on Heat Transfer and Cooling in Gas Turbines*, Antalya (Turkey), 12-16 October 1992, AGARD-CP-527, Paper 12.
5. G. Lodigiani, A. Trovati and L. Paci, "Cooling Geometry Optimization Using Liquid Crystal Technique", *Proceedings*

AGARD Conference on Heat Transfer and Cooling in Gas Turbines, Antalya (Turkey), 12-16 October 1992, AGARD-CP-527, Paper 13.

6. S.C. Cheah, H. Iacovides, D.C. Jackson, H. Ji and B.E. Launder, "LDA Investigation of the Flow Development Through Rotating Ducts", ASME Paper No. 94-GT-226, 1994.
7. T. Bo, H. Iacovides and B.E. Launder, "Convective Discretization Schemes for the Turbulence Transport Equations in Flow Predictions Through Sharp U-bends", *Intern. J. Numer. Method in Heat Fluid Flow*, Vol. 5, 1995, pp. 33-48.
8. H. Iacovides, B.E. Launder and H.-Y. Li, "The Computation of Flow Development Through Stationary and Rotating U-ducts of Strong Curvature", *Intern. J. Heat and Fluid Flow*, Vol. 17, 1996, pp. 22-33.
9. H. Iacovides, D.C. Jackson, G. Kelemenis, B.E. Launder, Y.M. Yuan, "Experiments on Local Heat Transfer in a Rotating Square-ended U-bend, *Intern. J. Heat and Fluid Flow*, Vol. 20, 1999, pp. 302-310.
10. O. Peroomian and S. Chakravarthy, "A Grid-Transparent Methodology for CFD", AIAA Paper 97-0724, Jan. 1997, Reno/NV.
11. O. Peroomian, S. Chakravarthy, S. Palaniswamy and U. Goldberg, "Convergence Acceleration for Unified-Grid Formulation Using Pre-conditioned Implicit Relaxation", AIAA Paper 98-0116.
12. U. Goldberg, O. Peroomian and S. Chakravarthy, "A wall-distance-free k-e model with enhanced near-wall treatment", ASME JFE, Vol. 120, 1998.
13. U. Goldberg, O. Peroomian, S. Palaniswamy and S. Chakravarthy, "Anisotropic k-e model for adverse pressure gradient flow", AIAA Paper 99-0152, Jan. 1999, 37<sup>th</sup> AIAA Aerospace Sciences Meeting, Jan. 1999, Reno/NV.
14. U. Goldberg, P. Batten, S. Palaniswamy, S. Chakravarthy and O. Peroomian,

"Hypersonic Flow Predictions Using Linear and Non-linear Turbulence Closures", publication scheduled in *J. Aircraft*, Vol. 37, no. 6, Nov.-Dec. 2000.

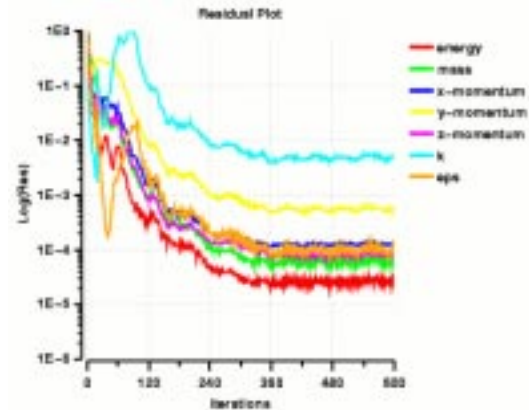


Fig.4 Residual history for stationary U-bend

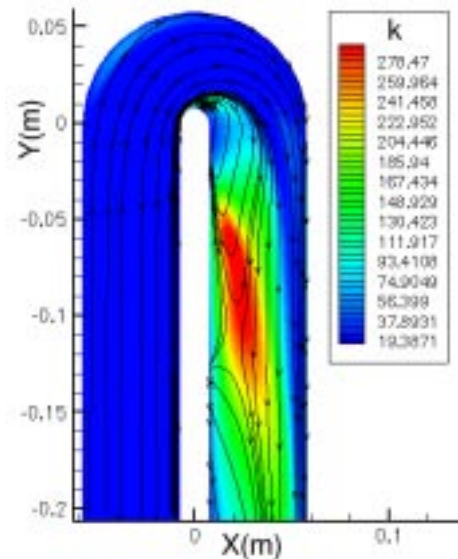
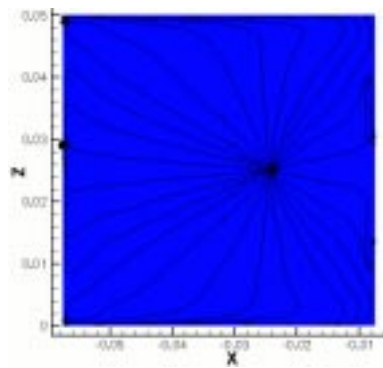
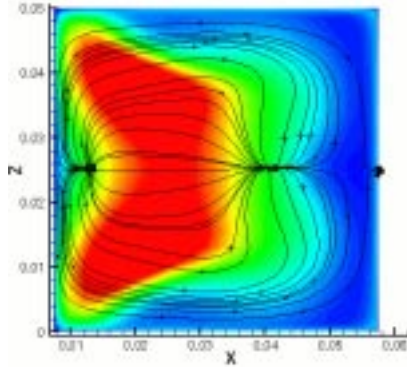


Fig. 5 Streamlines on symmetry plane for  $Ro=0$ .

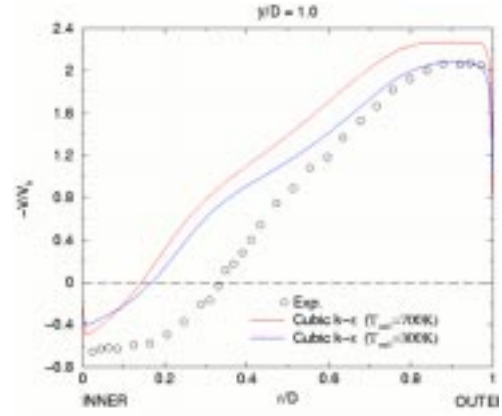


(a)

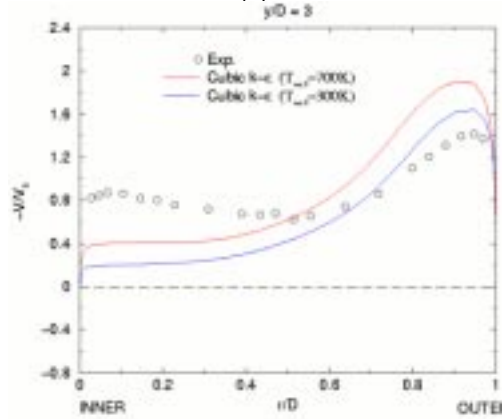


(b)

Fig. 6 Cross-flow in inflow and return pipes for stationary U-bend at  $y = -2D$  (a) inflow (b) return

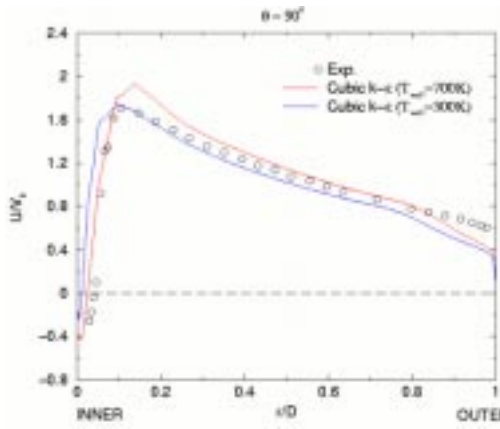


(c)

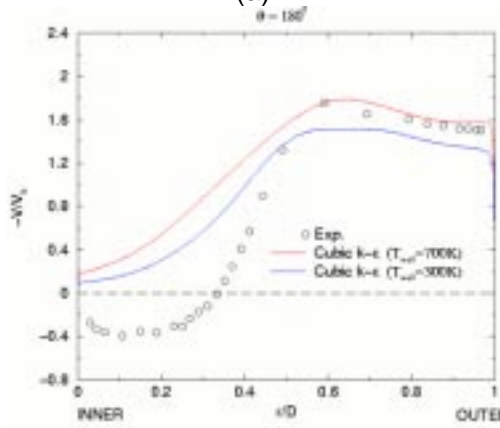


(d)

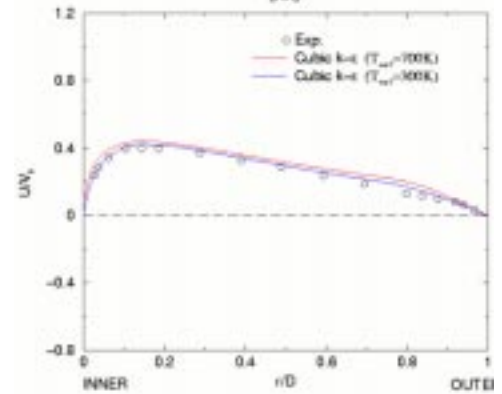
Fig. 7 Streamwise velocity component on symmetry plane of stationary U-bend at (a) 90 degree section, (b) U-bend exit, (c)  $y/D = 1$  and (d)  $y/D = 3$  downstream of the U-bend.



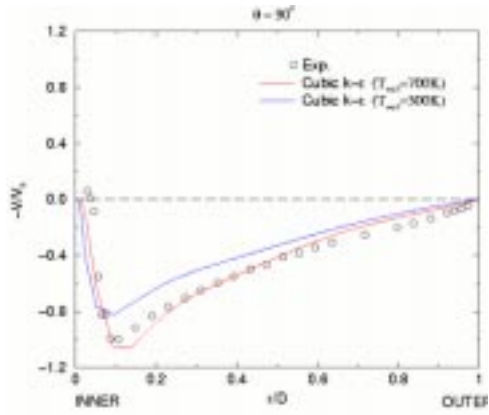
(a)



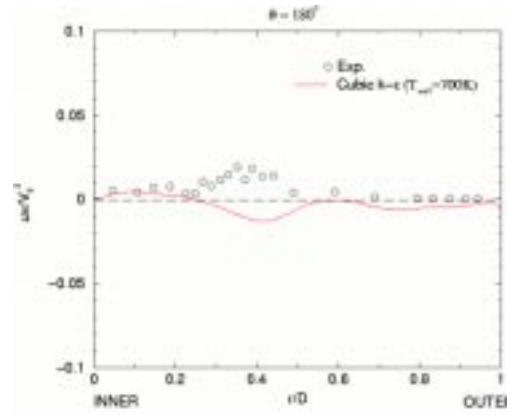
(b)



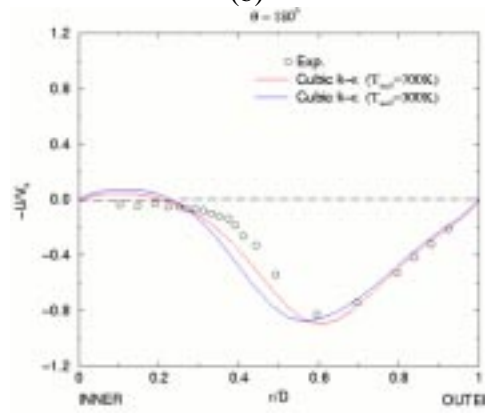
(a)



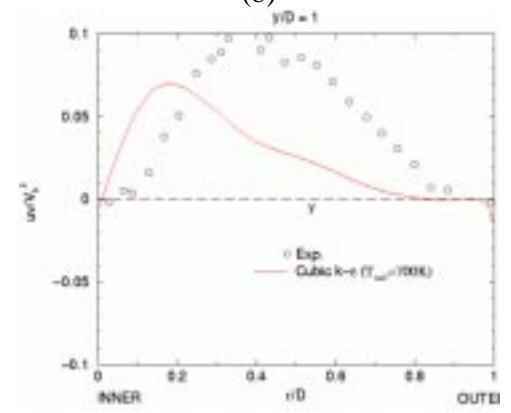
(b)



(b)



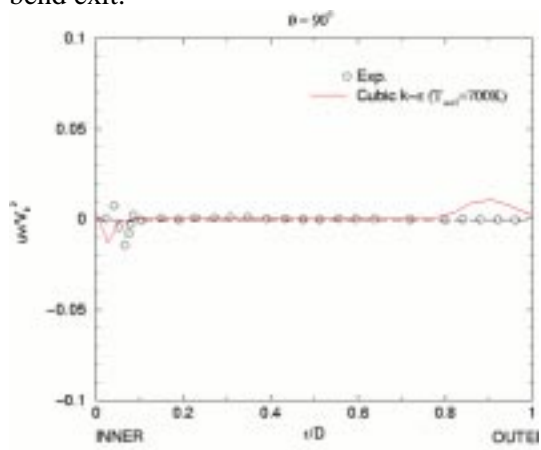
(c)



(c)

Fig. 8 Cross-stream velocity component on symmetry plane of stationary U-bend at (a) U-bend entry, (b) top of U-bend and (c) U-bend exit.

Fig. 9 Turbulence shear-stress on symmetry plane of stationary U-bend at (a) top of the U-bend, (b) exit section and (c)  $y/D=1$  downstream of U-bend.



(a)

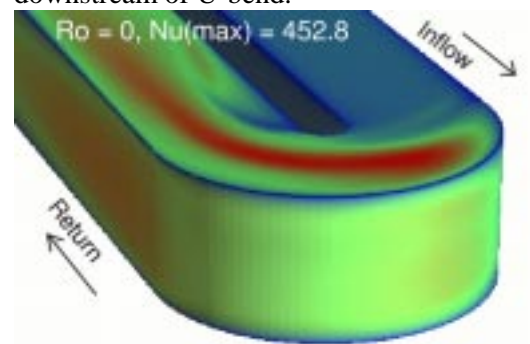


Fig. 10 Surface Nusselt number distributions for stationary U-bend.

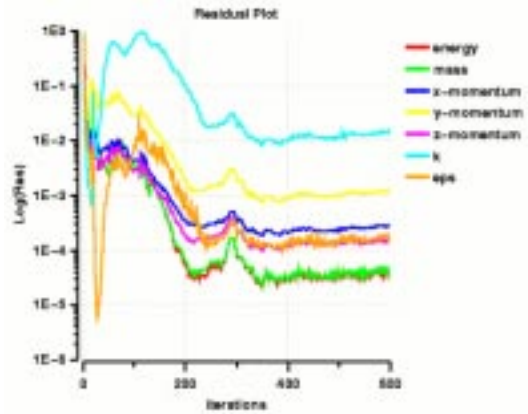


Fig.11 Residual history for  $Ro = 0.2$ .

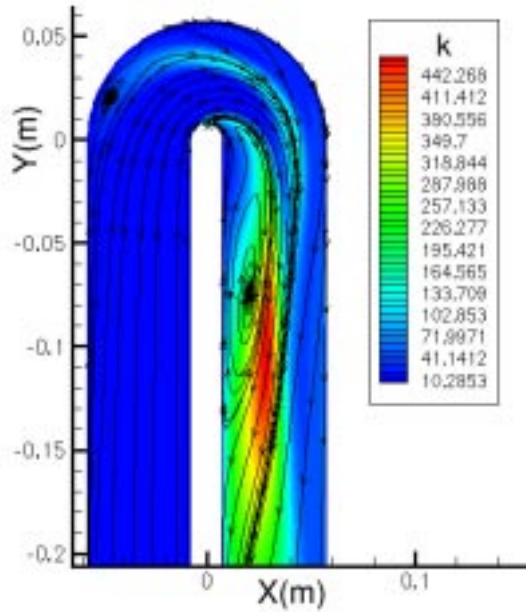
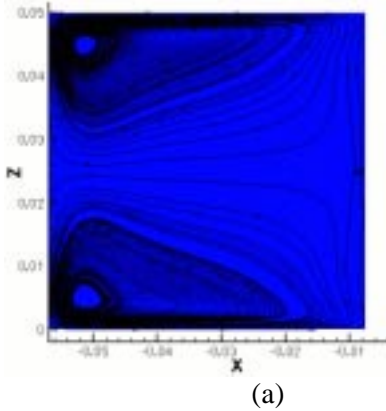
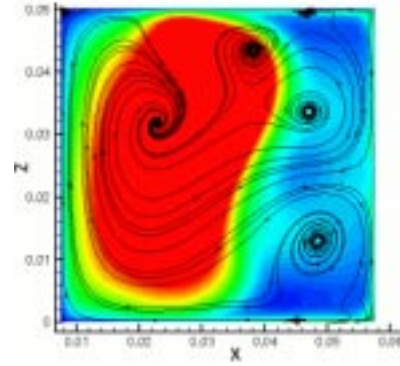


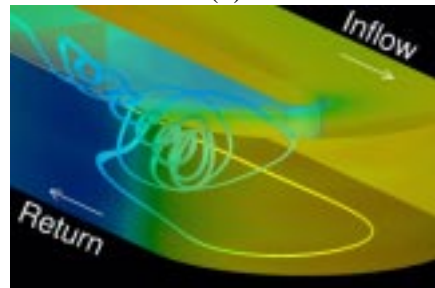
Fig. 12 Streamlines on symmetry plane for  $Ro = 0.2$ .



(a)

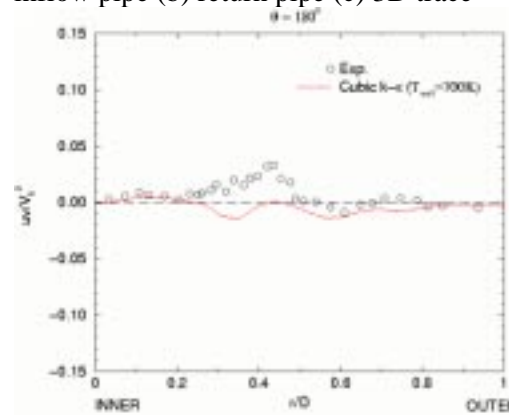


(b)

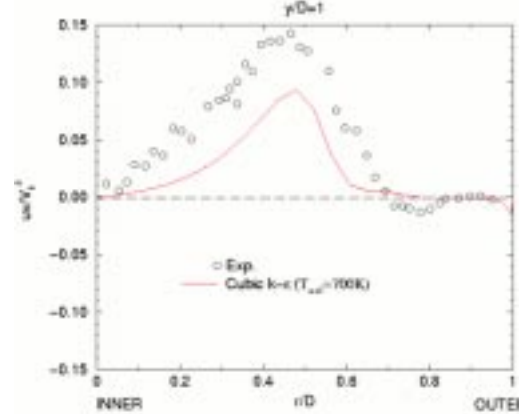


(c)

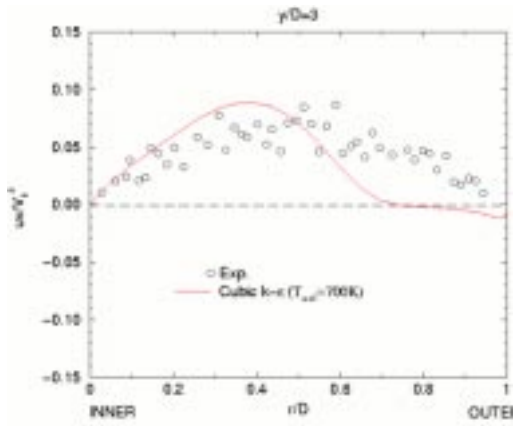
Fig. 13 Cross-flow for  $Ro = 0.2$  at  $y=-2D$  (a) inflow pipe (b) return pipe (c) 3D trace



(a)



(b)



(c)

Fig. 14 Turbulence shear-stress on symmetry plane of rotating U-bend ( $Ro = 0.2$ ) at (a) U-bend exit, (b)  $y/D = 1$  and (c)  $y/D=3$  downstream of U-bend.

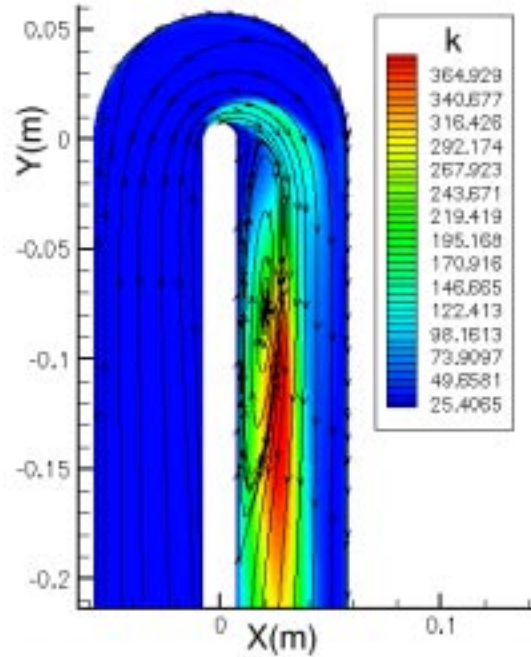


Fig. 17 Streamlines on symmetry plane for  $Ro = -0.2$ .

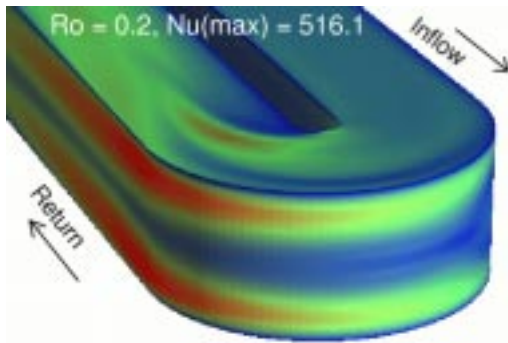


Fig. 15 Surface Nusselt number distributions for rotating ( $Ro=0.2$ ) U-bend.

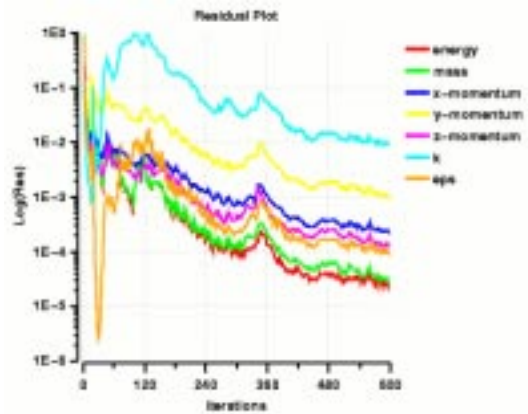
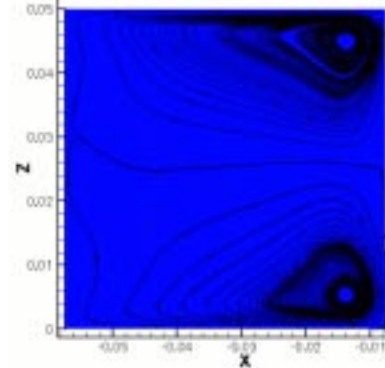
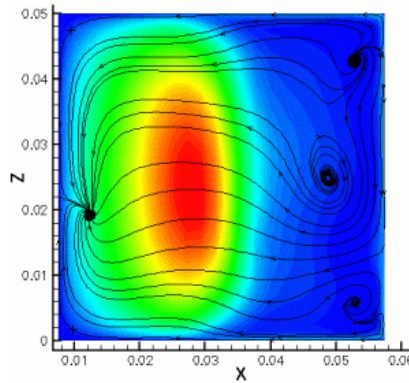


Fig.16 Residual history for  $Ro = -0.2$ .



(a)



(b)

Fig. 18 Cross-flow in inflow and return pipes for  $Ro = -0.2$  at  $y=-2D$  (a) inflow (b) return.

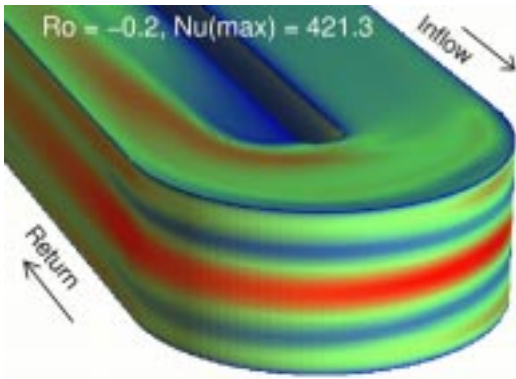


Fig. 19 Surface Nusselt number distributions for rotating ( $Ro = -0.2$ ) U-bend.

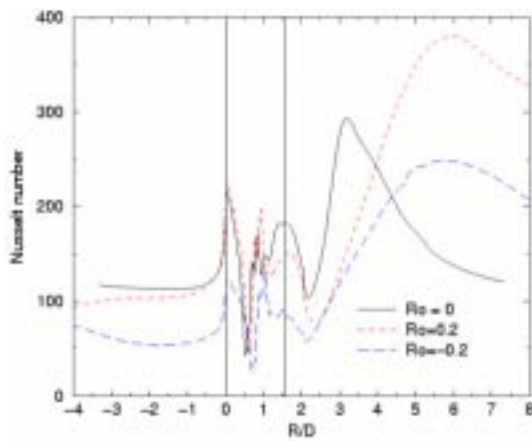


Fig. 20 Comparison of Nusselt number distributions on inner edge symmetry plane.

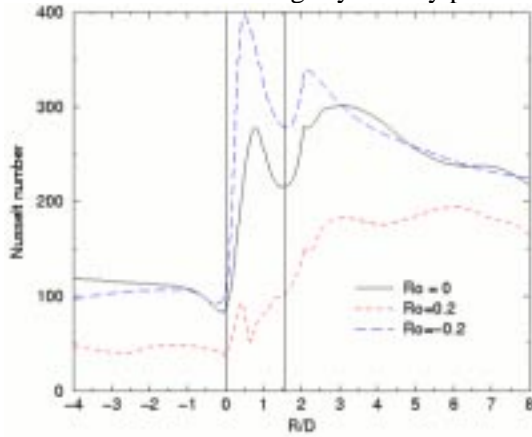


Fig. 21 Comparison of Nusselt number distributions on outer edge symmetry plane.